The Alborz Region: Identification of Seismogenic Nodes with Morphostructural Zoning and Pattern Recognition

A.I. Gorshkov[1], M. Mokhtari[2], and E.P. Piotrovskaya[3]

1. Prof., International Institute of Earthquake Prediction, Theory and Mathematical Geophysics, Moscow, Russia, e-mail: gorshkov@mitp.ru
2. Assistant Prof., Seismology Research Center, International Institute of Earthquake Engineering and Seismology (IIEES), Tehran, Iran
3. Assistant Prof., International Institute of Earthquake Prediction, Theory and Mathematical Geophysics, Moscow, Russia

ABSTRACT

In the Alborz region, we define seismogenic nodes prone to earthquakes M6+ and characteristic geomorphological-gelogical features that discriminate seismogenic nodes from non-seismogenic ones. Morphostructural nodes are formed around intersections or junctions of two or several lineaments. The nodes have been obtained by the morphostructural zoning (MZ) method. The compiled MZ map shows the hierarchical block-structure of the Alborz region, the network of boundary zones separating blocks, and the loci of the nodes, formed at the intersections of boundary zones. The recorded earthquakes of M6+ nucleate at some of the nodes. The pattern recognition algorithm CORA-3 defined other nodes capable of such size earthquakes using topographic, morphometric, and morphostructural parameters that describe the nodes. Nodes prone to M6+ exhibit the high topographic contrast and the increased fragmentation of the crust. Results of the work points out the high seismic potential of the Alborz region: this study identified a number of seismogenic nodes, where the target earthquakes have not yet been recorded.

Keywords:
Seismogenic nodes;
Alborz region;
Morphostructural zoning;
Lineaments

1. Introduction

In this work, the Alborz region located in northern Iran is studied. The Alborz mountain system extending for about 900km from the Lesser Caucasus in the west to the Kopet Dagh in the east reveals high level of seismic activity [1-6]. The goal of this work is to identify sites where earthquakes with $M \geq 6.0$ can occur and define the assemblage of geological-geomorphological features that discriminate such sites from areas of lower seismic potential.

The used methodology is quite different from the usual seismotectonic methods that allow to delineate seismogenic zones and calculate the seismic hazard inside these zones using probabilistic approach, e.g. [7-8]. The methodology we are using is based on the concept of the relationship between large earthquakes and morphostructural nodes, which are formed where morphostructural blocks are adjacent [9-10]. The methodology involves two steps. The first is to identify objects of recognition using the method of morphostructural zoning [10-11], with the objects being intersections of morphostructural lineaments. The second step uses pattern recognition algorithms to find those intersections where large earthquakes can occur [9-10].

The fact that earthquakes are nucleated at the nodes was first established in Central Asia by Gelfand et al [9]. Later on, Talwani [12] found that large intraplate earthquakes correlate with intersections of lineaments. He also proposed a model [13], which demonstrates that intersecting faults provide a location for stress accumulation. The relationship between earthquakes and intersections for plate boundaries and rift structures has been evidenced by Hudnut et al [14] and Gridlet and McConnell [15]. According to King [16], fault intersections provide locations for the initiation and healing of ruptures. Gabrielov et al [17] proposed a model implying that block interaction along intersecting faults leads to stress

and strain accumulation and secondary faulting around the intersection. This causes the generation of new faults of progressively smaller size, so that a hierarchical mosaic structure, essentially a node, is formed around the intersection. A procedure designed by Gvishiani and Soloviev [18] statistically proved the non-randomness of earthquake nucleation at the nodes.

The methodology has been systematically tested in many seismic regions of the world including California, Central Asia, Asia Minor, Caucasus, Mediterranean orogenic belts, Himalayas, Kamchatka and some others [19-33]. Recent earthquakes, in each of the regions previously studied with the methodology employed in this work, have proved that large earthquakes nucleate at the nodes. As Gorshkov et al [10] demonstrated, 90% of the post-publication events with relevant magnitudes occurred at the nodes. Among all post-publication earthquakes, 84% took place at the nodes recognized as capable of large earthquakes.

2. Tectonic and Topographic Setting

The Alborz mountain belt of northern Iran is a region of active deformation within the broad Arabia-Eurasia collision zone [34-37]. Initial collision of the northern promontory of Arabia with other continental blocks appears to have begun as early as the middle Eocene [38-39]. However, much of the broader collision zone did not start to deform until the mid-Miocene or later [40].

The Alborz accommodates the overall motion between the southern Caspian and central Iran, and seems to involve oblique left-lateral shortening. The Alborz mountain is roughly 900km long and 60-120km across, running along the southern side of the Caspian Sea. With its restricted width, the Alborz mountain is extremely steep, with the flanks abruptly joining the plains along major thrust faults on both sides [41]. The Alborz structures at both the eastern and western ends change in strike to pass into adjacent Talesh and Kopet Dagh fold and thrust belts. Geologically, this mountain range contains a thick sequence of Paleogene magmatic rocks and separate two independent marine sedimentary basins of South Caspian basin in the north and a Miocene basin in the south, e.g. [42-43]. Middle and upper Miocene marine clastics occur in the foothills in the northeast of the range. Miocene fluvial and lacustrine clastics are widespread in intermontane basins within the range and at its southern margin.

Structurally, the Alborz and Kopet Dagh is a stack of thrust sheets, produced by late Cenozoic active compressional deformation [39, 42]. Although the trend of the major structures varies from an *ENE* strike in the east to a *WNW* strike, prominent left-lateral strike-slip faulting occurs along the length of the Alborz.

Restoring the Eocene volcaniclastic Kahar Formation in central Alborz shows an estimate of ~25-30% *N-S* shortening; a finite contraction of about 30km [36]. Similarly, Berberian [44] estimates about 25% shortening of the Alborz over the last 5Myr. Dating of thermal histories of granites in the central Alborz indicate ~$0.7-1.4 mmyr^{-1}$ exhumation rate of central Alborz after 7Ma. This total late Neogene uplift of about 10km is nearly synchronous with subsidence in the south Caspian basin and onset of coarse molasses deposition in the Zagros fold-thrust belt [45]. According to *GPS* measurements in Central Alborz between 2000 and 2002, *N-S* shortening across the Alborz occurs at $5\pm2 mmyr^{-1}$. In addition, this mountain belt undergoes a left-lateral shear at a rate of $4\pm2 mmyr^{-1}$ [46].

Most of the well-constrained earthquake focal mechanisms show either reverse faulting or the range-parallel left-lateral strike-slip faulting, e.g. [41]. Evidence for left-lateral strike-slip faulting is substantial, involving up to 80km of coseismic left-lateral rupture of the 1990.06.20 (*Mw* 7.3) Rudbar-Tarom earthquake and the 1970.07.30 Karnaveh earthquake, *Mw* 6.4, [47]. Once again, there is abundant evidence for recent uplift in the Alborz, in the form of incised river terraces and coastal marine terraces [44].

The present-day topography of the Alborz region has been strongly affected by tectonics, and by neotectonics in particular. The formation of the Alborz orogen has been started in Paleocene, while most young deformations that built the present-day topography took place in Pliocene - Quaternary [39, 48-50]. The rugged Alborz mountains, extend laterally 900km around the south Caspian sea. The Alborz has an average elevation of nearly 3000m and includes three of the highest points in Iran. The range is higher than the neighboring Talesh and Kopet Dagh, with many summits in the range of 3600-4800m, culminating in the Quaternary volcano of Damavand.

3. Methodology

Two principal steps compose the methodology. The first step is the delineation of the objects of the analysis-the morphostructural nodes-by the

morphostructural zoning (*MZ*) method. The second is the classification of all mapped nodes, by the pattern recognition algorithm *CORA*-3, into nodes where earthquakes with magnitude exceeding a certain threshold are possible and nodes where only earthquakes with smaller magnitude may happen. Here only the basic definitions necessary for the understanding of the results are described.

3.1. Morphostructural Zoning Method

Modern geophysics considers a hierarchical dynamic system of lithospheric blocks and their boundaries as the supporting medium of earthquakes [51-55]. Blocks of different scale, boundary zones and nodes are major components of a complex hierarchical system of the lithosphere [53]. Therefore, delineation of block-and-fault geometry for a seismic region is a necessary stage in studying earthquake prone areas. In order to delineate the block-structure of the Alborz region, we employ the morphostructural zoning (*MZ*) method that was designed for identification of seismogenic nodes [10, 11, 29].

The present-day topography of the study region is the main subject of the analysis in *MZ*. It should be emphasized that *MZ* does not use the information on the locations of earthquakes in the study region.

By the *MZ* the study region is divided into a system of hierarchically ordered areas, characterized by homogeneous present-day topography and tectonic structure. *MZ* distinguishes (1) blocks (areas) of different rank; (2) their boundary zones, morphostructural lineaments; and (3) sites where lineaments intersect, the nodes. All components of the hierarchical system compose a single system. A morphostructural lineament is viewed as a boundary zone between territorial units delineated by *MZ*. The rank of the lineament is determined by the rank of a territorial unit bounded by it.

MZ differs from the standard morphostructural analysis (e.g. [56]) where the term "lineament" [57] is used to define the complex of alignments detectable on topographic maps or on satellite images. According to that definition the lineament is locally defined and the existence of the lineament does not depend on the surrounding areas. In *MZ*, the primary element is the block - a relatively homogeneous area, while the lineament is a secondary element of the morphostructure. The borders of the blocks form the lineaments. This means that the existence and the position of the lineaments are determined not locally, but as a part of a broad pattern. If a certain alignment does not separate

two topographically different areas, that alignment cannot be viewed as a lineament in *MZ*, therefore, the lineaments are secondary features with respect to the blocks.

MZ hierarchically orders blocks and lineaments assigning them ranks from the highest to the lowest. Lower rank blocks are parts of a higher rank block. Usually, three levels of a hierarchy were considered in different regions. Blocks of the first rank, mountain countries, are divided into blocks of the second rank, megablocks. Megablocks are further divided into blocks of the third rank, called blocks per se.

The uniformity of each morphostructural unit is determined by a certain set of morphometric features and their quantitative index [10].

A morphostructural lineament is viewed as a boundary zone between territorial units delineated by *MZ*. There are no morphostructural lineaments in the absence of a recognized territorial unit (a block). *MZ* distinguishes longitudinal and transverse lineaments.

Longitudinal lineaments follow the boundaries of large topographic forms or slopes of composite ranges. They usually include zones of the prominent faults and, in general, are more evident than transverse lineaments. Transverse lineaments go across the predominant trend of topography and tectonic structures. Normally, they appear discontinuously on the Earth' surface. Zones of transverse lineaments are traced along tectonic scarps, faults, flexures and narrow intrusive bodies, linear contacts in rocks, and rectilinear segments of river valleys, that are usually fault-dominated in tectonically active mountain systems belonging to the Alpine-Himalayan belt [58-59].

The rank of the lineament depends on the rank of block by the lineament. Higher rank lineaments include the wider zone of deep-seated deformation. For instance, Gvishiani et al [60] for the Caucasus and Cisternas et al [19] for the Western Alps demonstrated that first and second rank lineaments correlate with considerable changes in the thickness and in the configuration of Moho discontinuity, while third rank lineaments correspond to the escarpments in the crystalline basement.

Morphostructural nodes are formed around intersections or junctions of two or several lineaments. A node may include more than one intersection or junction. Lineament zones become wider at nodes. Nodes are characterized by a mosaic combination of various topographic forms and by an increased number of linear landforms of various strikes that

reveal instability of the area. River valleys within the nodes are represented by rectilinear segments of various strikes. Knee-like bends are characteristic of the river streams within a node. There are oblique segments of valleys that are discordant with respect to the direction of the maximum gradient. Excessive concentration of water (streams, springs) at nodes has to be noted. This is because the confluence of several rivers confined to the crossings of lineaments, as well as to the uplift of underground waters, in particular thermal springs.

The size and geometry of a node can be outlined with fieldwork. The sizes of nodes range drastically and depend on the number of intersections or junctions that form a node as well as on the number of lineaments and their ranks. If no field investigations were made, the circle of a certain radius can be used as a substitute for a node. The radius of the circle depends on the size of the target earthquakes.

3.2. Pattern Recognition Applied to Identification of Earthquake-Prone Areas

The nodes delineated with morphostructural zoning are used as objects of recognition. Each object is described by an uniform set of topographical, geological, and geomorphological parameters. These descriptions are vectors whose components are the values of the parameters.

Thus, the pattern recognition problem consists of assigning the vectors to two classes: vectors **D** (historically stands for "Dangerous") representing nodes where earthquakes with $M \geq M_0$ can occur and vectors **N** (stands for "Not dangerous") describing nodes where only earthquakes with $M < M_0$ can happen. The classification is known for some objects of recognition on the basis of the seismic history recorded in the study region. These objects form a training set of vectors that belong to known classes. The training set consists of vectors **D₀** and **N₀** that represent, respectively, the nodes where strong earthquakes occurred and the nodes that are far from the known epicenters of such earthquakes. A pattern recognition algorithm provides a classification of the vector space into **D** and **N**.

Nodes are characterized by a set of topographic, geological and geophysical parameters. A vector of values of these parameters represents each node. The set of these vectors is the input for the *CORA*-3 pattern recognition algorithm that we use in this study.

Application of the *CORA*-3 algorithm includes the following two stages:

1) Learning stage - selection of the distinctive features of each class on the basis of the training set composed by **D₀** and **N₀** subsets, which are constituted by all the sample nodes representative of the classes **D** and **N**, respectively;
2) Classification stage - determination of the class to which each node belongs.

The distinctive features (characteristic traits) for classes **D** and **N** are selected at the learning stage as follows.

Let *l* be the number of components of the binary vectors representing the node. The trait is a matrix **A** defined as:

$$\mathbf{A} = \begin{Vmatrix} i_1 & i_2 & i_3 \\ \delta_1 & \delta_2 & \delta_3 \end{Vmatrix},$$

where i_1, i_2, i_3 are natural numbers, such that $1 \leq i_1 \leq i_2 \leq i_3 \leq l$ and δ_1, δ_2 and δ_3 are equal to 0 or to 1. A node (binary vector) numbered i, $\mathbf{i} = (\omega_1^i, \omega_2^i, ..., \omega_1^i)$ posses the trait **A** if:

$$\omega_{i_1}^i = \delta_1, \ \omega_{i_2}^i = \delta_2, \ \omega_{i_3}^i = \delta_3.$$

The characteristic traits are selected with four parameters of the algorithm $k_1, \bar{k}_1, k_2, \bar{k}_2$, which must be integer non-negative values. Let *W* be the set of all the nodes considered and $K(W, \mathbf{A})$ the number of nodes $\omega^i \in W$ that posses the trait **A**. The trait **A** is a characteristic trait of class **D**, when $K(\mathbf{D}_0, \mathbf{A}) \geq k_1$ and $K(\mathbf{N}_0, \mathbf{A}) \leq \bar{k}_1$, and the trait **A** is a characteristic trait of class **N**, when $K(\mathbf{N}_0, \mathbf{A}) \geq k_2$ and $K(\mathbf{D}_0, \mathbf{A}) \leq \bar{k}_2$.

The classification is made as follows. For each node ω^i the algorithm calculates the number n_D^i of the characteristic traits for class **D**, the number n_N^i of those for class **N**, and the difference $D_i = n_D^i - n_N^i$. Class **D** includes the nodes ω^i for which $D_i \geq D$, while class **N** includes the nodes for which $D_i < D$. *D* as well as $k_1, \bar{k}_1, k_2$, and $\bar{k}_2$ is a parameter of the algorithm.

4. Morphostructural Zoning of the Alborz Region

The set of recognition patterns and nodes has been obtained with the help of morphostructural zoning. The morphostructural map of the Alborz region, which shows the loci of nodes has been compiled on the basis of joint analysis of topographic, geological, tectonic, and seismotectonic maps of Iran at different scales as well as the *LANDSAT* photos.

4.1. Moprphostructural Units Delineated in the Alborz

First Rank Morphostructures: According to the principles of *MZ*, we consider the Alborz as a single

mountain country created by the Alpine orogenesis [39, 48]. First rank lineaments shown in Figure (1) separate the Alborz from the surrounding large-scale geotectonic domains. These lineaments have been traced along the topographically contrasting junctions of mountain ranges composing the Alborz with the neighboring plateaus or basins. In the north, longitudinal first rank lineament from 1 to 99 delimits the Alborz and the Caspian lowland, see Figure (1). The lineament is traced along the northern foot of the Alborz. The section of the lineament from 1 to 11 includes the Talesh fault and the fragment of the lineament from 11 to 99 corresponds to the Khazar fault. In the west, first rank lineament from 1 to 12 separates the Alborz from the Talesh mountains and from volcanic areas in the Lesser Caucasus; the lineament includes the Sangavar fault [61]. The southern boundary, the lineament from 12 to 100 of the broken configuration, separates the Alborz mountain belt from the Central Iranian Basins and the Great Kavir. In the east, the transverse lineament from 99 to 100 divides the Alborz and the Kopet Dagh mountains. Figure (1) shows the correlation of the first rank lineaments with major active faults delineated by Hessami et al [61].

Second Rank Morphostructures: Seventeen megablocks shown in Figure (2) have been outlined in the Alborz region due to the difference in the elevation and orientation of individual ranges composing the mountain belt. The second rank lineaments bound megablocks. The longitudinal segmentation of the Alborz into megablocks is controlled by longitudinal second rank lineaments that correspond to the prominent faults shown on geological map of Iran. The transverse subdivision of the mountain belt is dominated by transverse lineaments of the second rank. Figure (2) shows the correlation of the second rank lineaments with major active faults delineated by Hessami et al [61].

As it is seen in Figure (2) transverse lineaments control the geometry of the Alborz orogen. Additionally, most of them shift the foot-line of the Alborz causing displacements in the configuration of the first rank lineaments that bound the mountain belt.

Transverse lineament from 5 to 7 controls the change in orientation of the axis of the Alborz ridge from the *N-S* direction in megablock *I* to the *NW-SE* trend in megablock *II*. In relief the lineament is expressed by a system of river valleys of a near *E-W* orientation.

Transverse lineament from 8 to 16 that corresponds to the Masuleh fault follows along the Rud-e Qezel Uznan river valley [61]. It separates two huge ranges of different elevation and orientation, the Boghrov Dagh range in megablock *II* and the Kuh-e Anguran range in megablock *III*.
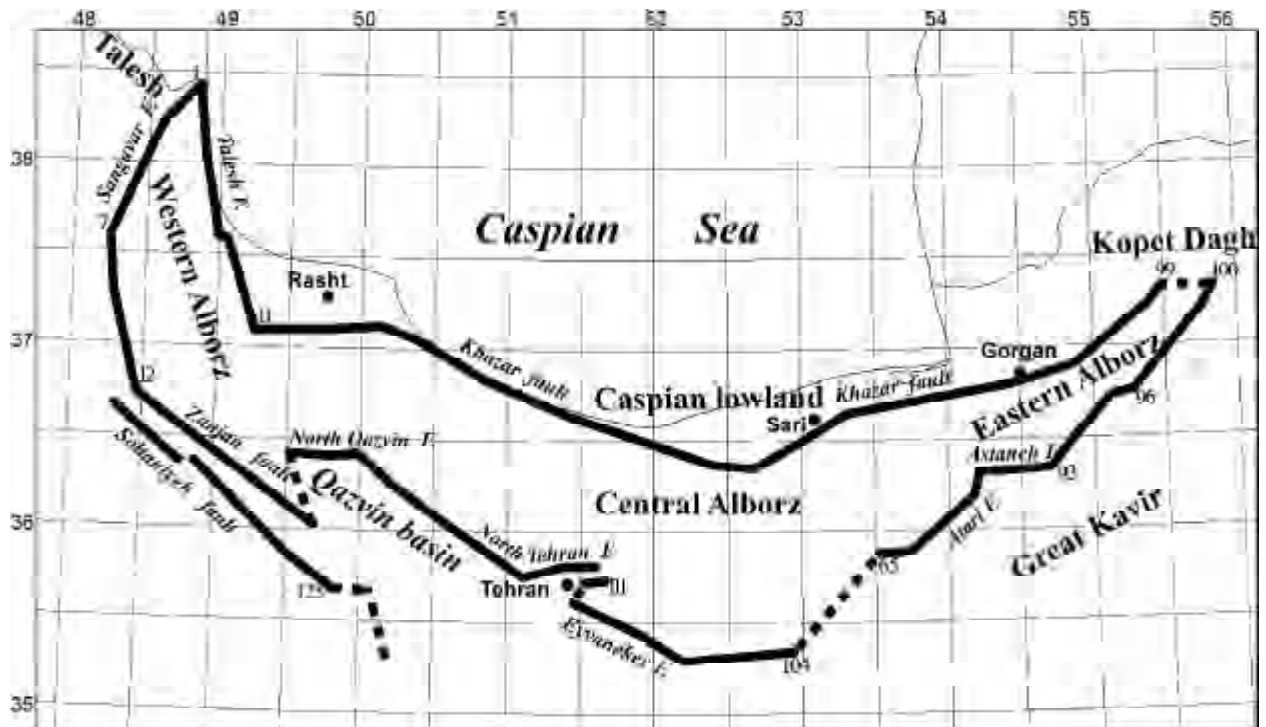

Figure 1. First rank morphostructures delineated in the Alborz region. Thick lines denote the lineaments of the first rank. Continues lines depict the longitudinal lineaments, while the discontinuous ones represent the transverse lineaments. The numbers indicate lineament intersections.
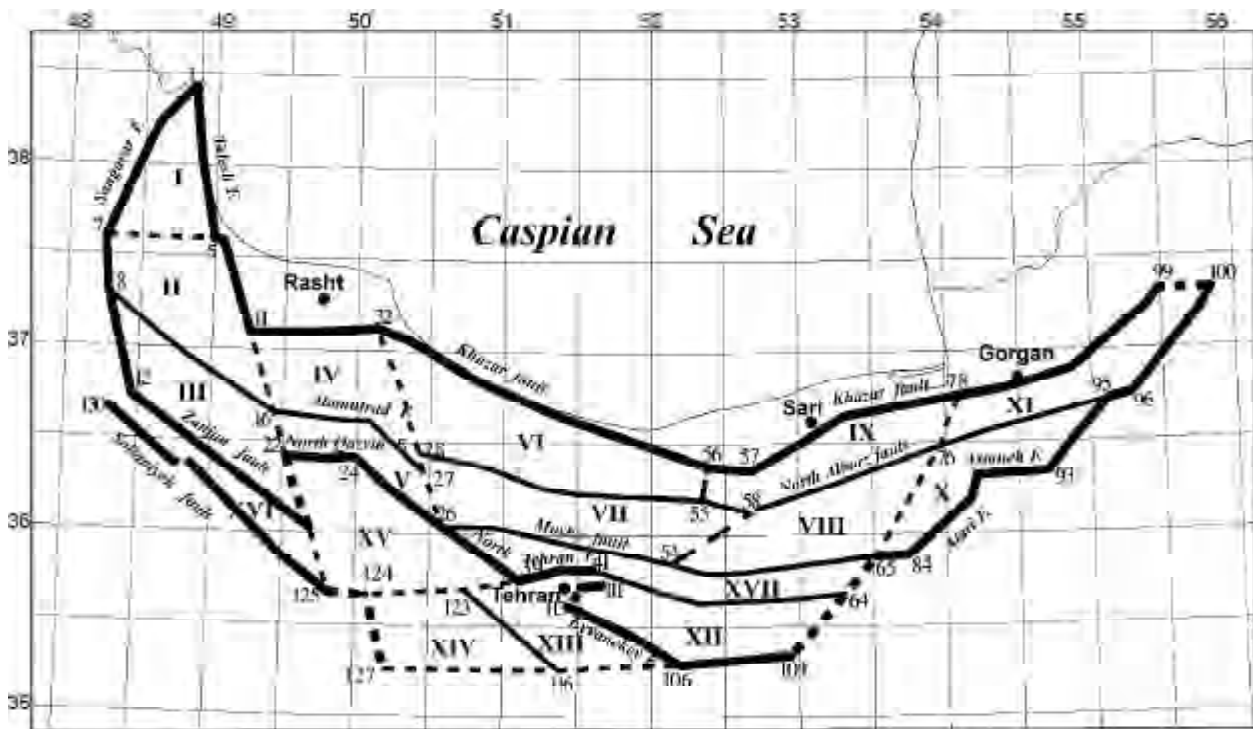
Figure 2. Second rank morphostructures in the Alborz region. Thick lines denote the lineaments of the first rank. Medium lines show lineaments of the second rank. Continues lines depict the longitudinal lineaments, while the discontinuous ones represent the transverse lineaments. Romanian numbers indicate the megablocks, while the other numbers present the lineament intersection.

The lineament from 11 to 22 is the southward extension of the Talesh fault appears to be a very important structural boundary between the Western and Central Alborz since it controls the sharp change in the orientation and morphology of the Alborz mountain belt. In Western Alborz the tectonic structures and large ridges exhibit *NW-SE* trend, while in east of it, in the Central Alborz, the tectonic structures and large ridges stretch in near *E-W* direction. Additionally, the axes of the ridges east of this line are remarkably shifted southward with respect to the axes of the ridges west of it suggesting right-lateral displacements along the lineament. The lineament is traced along the near *N-S* rectilinear lengths of the river valleys including knee-like bend of the Rud-e Qezel Uznan river. The southward extension of the lineament, first rank lineament from 22 to 23, shifts the foot-line of the Alborz southward. The lineament is traceable further to the south where it separates the Zanjan range and the Qazvin alluvial basin.

The Central Alborz was divided into three transverse segments due to the difference in elevation in it western, central and eastern parts. The lineament from 26 to 32 separates western segment (megablocks *V* and *VI*) from most elevated central part of the Alborz (megablocks *VI* and *VII*). In relief the

lineament is marked by steep escarpments on the slopes of the ridges and by linear fragments of river valleys including knee-like bend of the Teleghan Rud river. A system of transverse second rank lineaments that includes the lineaments from 54 to 58, from 58 to 59, and from 58 to 57 separates the relatively lowered part of the Central Alborz (megablocks *VIII* and *IX*). These lineaments control the changes in the morphology of the Central Alborz; east of the lineament relief is of the lesser contrast and the northern flank of the Alborz gently grades into the flat Caspian lowland.

The boundary between the Central and Eastern Alborz, lineament from 65 to 78, is traced along the *NE-SW* linear fragment of the Rud-e Tejen river and its northern tributary of the same orientation. Along the lineament the Seyan Kuh and Kuh-e Mantab ridges on the southern flank of the Alborz are shifted to the north suggesting left-lateral displacements.

The geometry of megablocks defined by morpho-structural zoning suggest that the Western Alborz, composed by megablocks *I*, *II*, and *III*, as well as the Eastern Alborz, included megablocks *X* and *XI*, are shifted to the north with respect to the Central Alborz along transverse lineament from 11 to 22 and transverse lineament from 65 to 78, respectively.

Longitudinal lineaments of the second rank are

more evident in the present-day topography of the Alborz. These lineaments separate mainly large isolated ridges or the assemblages of the ridges; they were traced along the extensive fault-dominated longitudinal river valleys and most of them correspond to major tectonic faults mapped by Hessami et al [61].

Within considered part of the Iranian Plateau south of the Alborz we have delineated megablocks *XIII-XVI*. Each of them includes basin filled with Neogen-Quaternary deposits. These basins differ in altitude of their bottoms, see Table (1). Megablock *XIII* includes part of the Dashte-Kavir basin, mega-block *XIV* corresponds to the Qum basin, megablock *XV* the embraces the Qazvin basin, and megablock *XVI* includes the Zanjan basin.

Table 1. Earthquakes with M ≥ 6.0 in the Alborz region.

Year	Month	Day	Depth	Latitude	Longitude	*Ms*
C.3000-	-	-	-	36.82	49.48	>7
C.4500BP	-	-	-	36.70	49.98	>6.5
C.38.500-	-	-	-	35.82	52.11	>6.5
C.1.800	-	-	-	36.11	50.78	>7
C.312-280BC	-	-	-	35.50	51.80	7.6
743	-	-	-	35.30	52.20	7.20
855-856	-	-	-	35.60	51.50	7.10
856	12	22	-	36.10	54.20	8.10
864	1-2	-	-	35.80	51.40	6.50
874	11-12	-		37.16	55.28	6.00
958	2	23	-	36.00	51.00	8.00
1052	-	-	-	36.60	50.30	6.80
1119	12	10	-	35.80	49.90	6.50
1127	-	-	-	36.30	53.60	6.80
1177	5	-	-	35.70	50.70	7.20
1301	-	-	-	36.10	53.20	6.70
1485	8	15	-	36.70	50.30	7.20
1498	-	-	-	37.20	55.20	6.50
1608	4	20	12	36.40	50.50	7.60
1639	-	-	-	36.60	50.00	6.10
1665	-	-	-	35.70	52.10	6.50
1678	2	3	6	37.20.	50.00	6.50
1687	-	-	-	36.30	52.60	6.50
1809	-	-	-	36.33	52.60	6.50
1825	-	-	-	36.10	52.60	6.70
1830	3	27	-	35.73	52.28	7.10
1863	12	30	22	38.20	48.60	6.10
1890	7	11	7	36.60	54.70	7.20
1896	1	4	-	37.7	48.32	6.70
1905	1	9	6	37.00	48.70	6.20
1935	3	5	10	36.25	53.25	6.00
1935	4	11	23	36.50	53.50	6.75
1957	7	2	0	36.10	52.70	7.00
1962	09	01	19	35.60	49.90	7.20
1978	11	4	15	37.67	48.91	6.40
1980	5	4	18	38.05	48.49	6.60
1985	10	29	20	36.36	54.77	6.10
1985	10	29	13	36.68	54.77	6.00
1990	01	12	18	35.90	52.98	6.00
1990	6	20	21	36.99	49.22	7.40
2004	5	28	12	36.177	51.569	6.30

Third rank morphostructures: The present-day relief in the Alborz is very heavily dissected. Over the mountain chain, the quantitative index of the topography changes sharply within short distances, therefore *MZ* allowed for a dense network of third rank lineaments. Specifically, this is true for eastern part of the Alborz. These lineaments have been traced along the steep scarps on the slopes of the ridges and along the rectilinear fragments of river valleys that are usually fault-dominated in young mountains to which belongs the Alborz too.

In total, with *MZ*, 134 intersections of lineaments in the Alborz region are outlined, see Figure (3). Each of them is considered as a node.

4.2. Nodes and Large Earthquakes

Since the nodes have been outlined from the cartographic sources without field investigations, their size and shape have not been defined. Here, like in other regions studied with the same methodology, e.g. [31-33], we define the node as a circle of 25km of radius, centered at the point of intersection of the lineaments. Using this formal node definition, each point of lineament intersection is a node but, in reality, two or three closely situated intersections may belong to the same node. Such node dimension is in agreement with the size of earthquake source for the magnitude range considered in this work. According to Wells and Coppersmith [62], the source size of an earthquake with *M* = 6.0 is about 20km in length and 10km in width.

In this work, we recognize the nodes capable of earthquakes with *M* ≥ 6.0 and used available earthquake catalogs [63-65] in order to select the sample nodes hosting events of the target size for the learning stage of the recognition,

The selected earthquakes are presented in Table (1) and plotted in Figure (4). As it can be seen in Figure (4), the epicenters of the earthquakes considered are located near the intersection of lineaments, i.e. at the nodes. The distance between the epicenters and the points of intersections does not exceed 25km, i.e. the recorded earthquakes nucleate at nodes.

5. Recognition of Nodes Prone to Earthquakes with M ≥ 6

The recognition of the nodes has been performed with the *CORA*-3 algorithm. The goal of the recognition is to classify all the nodes delineated in the Alborz region into the two classes:
1) Class **D** containing the nodes where earthquakes

with magnitude $M \geq 6.0$ may occur;

2) Class **N** containing the nodes where only earth-quakes with $M < 6.0$ may occur.

Application of the *CORA*-3 algorithm involves two stages:

1) Learning stage - search of the distinctive features of each class on the basis of the training set composed by $\mathbf{D}_0$ and $\mathbf{N}_0$ subsets, which are constituted by all the sample nodes representative of the classes D and N, respectively;
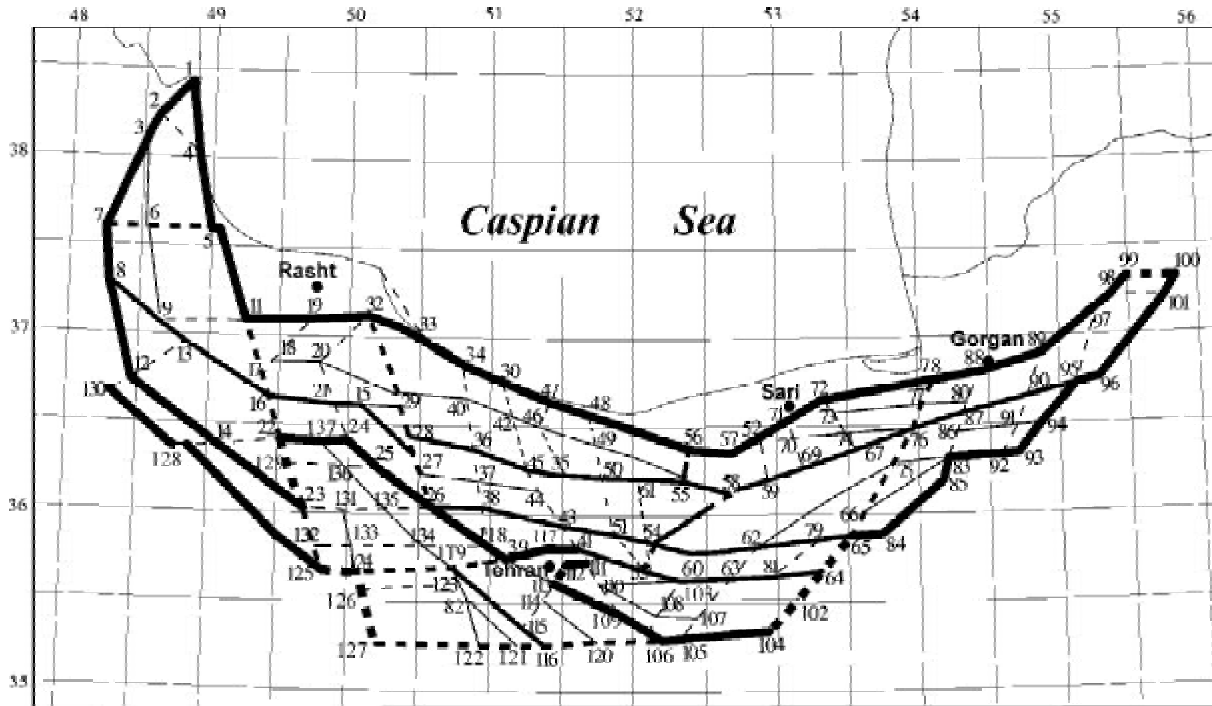

Figure 3. Morphostructural map of the Alborz region. Thick lines indicate the lineaments of the first rank; medium lines show lineaments of the second rank; thin lines depict the lineaments of the third rank. Continues lines depict the longitudinal lineaments, while the discontinuous ones represent the transverse lineaments. The numbers are the intersections of lineaments.
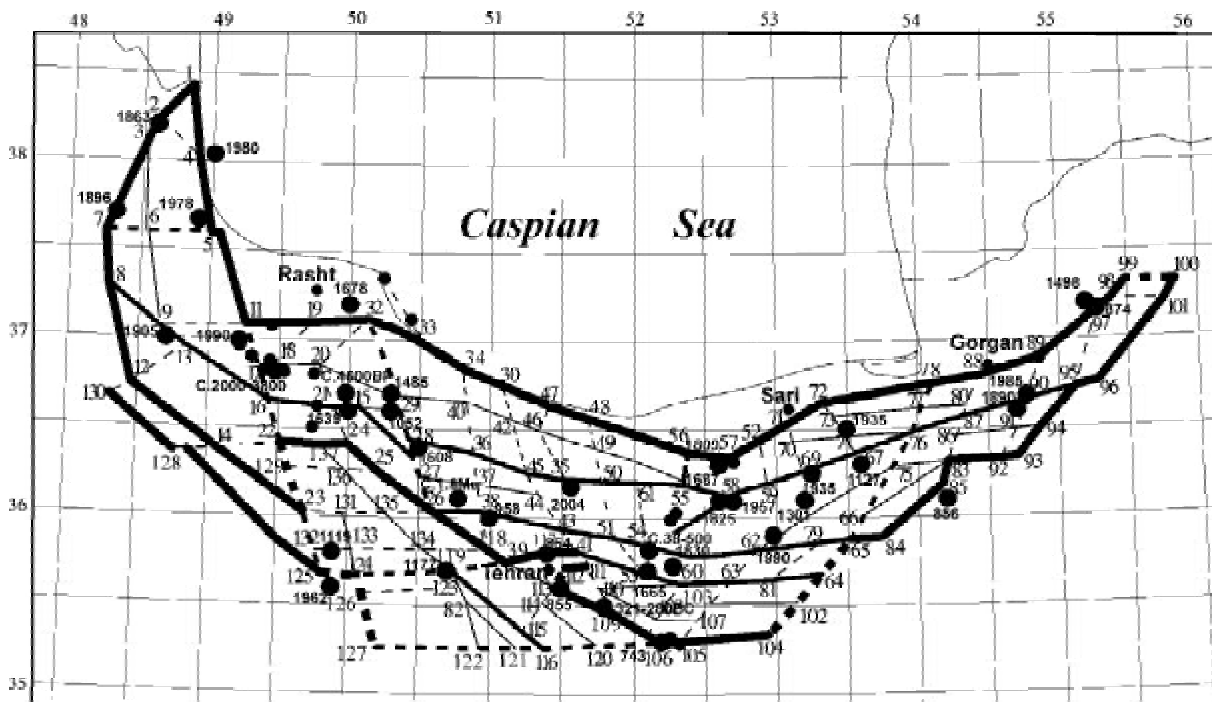

Figure 4. The spatial correlation between the nodes and earthquakes with M ≥ 6.0. Lines and numerals are the same as in Figure (3.) Larger dots mark epicenters of earthquakes with M ≥ 6.0. Smaller dots show earthquakes M ÷ 5.0-5.9.

2) Classification stage - determination of the class to which each node belongs.

5.1. Selection of the Training Sets for the CORA-3 Algorithm

At the learning stage 134 nodes, delineated in the study region, are a priori divided into three sets: $\mathbf{D}_0$, $\mathbf{N}_0$, and $\mathbf{X}$.

To assemble $\mathbf{D}_0$, we have been looking for the nodes situated most closely to the epicenters of earthquakes with $M \geq 6.0$ shown in Figure (4).

On the contrary, to form $\mathbf{N}_0$, the nodes that are most distant from the epicenters of earthquakes with $M \geq 6.0$ are sorted out in Figure (4) and, to be conservative, from smaller events with $5.0 \leq M < 5.9$ as reported by Engdahl et al [63].

As a result, 33 nodes out of the 134 delineated in the Alborz have been included in $\mathbf{D}_0$: 2, 4, 5, 7, 9, 11, 15, 17, 20, 21, 26, 28, 29, 32, 35, 38, 53, 54, 57, 58, 60, 67, 69, 74, 85, 90, 97, 106, 109, 113, 117, 119, 125.

The subset $\mathbf{N}_0$ contains 70 nodes: 1, 6, 8, 10, 12, 14, 22, 23, 25, 30, 34, 36, 39, 40, 42, 43, 44, 45, 46, 47, 48, 49, 51, 52, 59, 61, 62, 63, 64, 65, 66, 70, 71, 72, 76, 77, 78, 79, 80, 81, 82, 83, 84, 86, 87, 88, 92, 93, 94, 96, 99, 100, 101, 102, 103, 104, 107, 108, 115, 116, 118, 120, 121, 122, 127, 129, 130, 131, 132, 135, 136.

The remaining 31 nodes (3, 13, 16, 18, 19, 24, 27, 33, 37, 41, 50, 55, 56, 73, 75, 89, 91, 95, 98, 105, 110, 111, 112, 114, 123, 124, 126, 128, 133, 134, 137) are not included in the training set because they are neither close enough to the relevant epicenters nor sufficiently distant from them. They were assigned to the set $\mathbf{X}$ that is not employed for the search of the characteristic traits. The nodes from the set $\mathbf{X}$ have been classified at the recognition stage.

5.2. Parameters of the Nodes Used for Recognition and Their Discretization

A uniform parameterization of the nodes in the form of a common questionnaire is needed to apply the *CORA*-3 algorithm. The algorithm operates with vectors of parameters representing nodes. The accumulated experience in recognizing earthquake-prone areas [10] has established the following sets of parameters as typical:

- A multitude of parameters describing topography;
- Parameters describing the complexity of lineament-and-block geometry in the study region;
- Parameters describing gravitational field anomalies.

In principle, all available information related directly or indirectly to the level of seismic activity can be used to characterize the objects of recognition. The only necessary pre-condition for the use of a parameter is the availability of uniform measurements across the entire study region.

Here, the parameters listed in Table (2) are used. All of them have been employed for the recognition of earthquake-prone areas in previous investigations. Among the many other parameters, that have been tested, the parameters listed in Table (2) have been found sufficiently informative to discriminate the seismogenic nodes from non-seismogenic ones (see the review of this problem by Gorshkov et al [10]). The parameters describing the topographic altitudes and the area of soft sediments characterize indirectly the contrast and intensity of the present-day tectonic movements, while those describing the lineament-and-block geometry can be related to the degree of crust fragmentation. The values of the parameters have been measured within each node, i.e. inside a circle with 25km of radius, from available topographic and geological maps as well as from the *MZ* map of the Alborz region, see Figure (3).

Table 2. Parameters used for the recognition and thresholds of their discretization.

Parameters	Thresholds of Discretization
A) Topographic parameters	
Maximum topographic altitude, m, (Hmax)	2696 3400
Minimum topographic altitude, m, (Hmin)	280 1100
Relief energy, m, (DH) (Hmax - Hmin)	2379
Distance between the points Hmax and Hmin, km (L)	38
Slope, (DH/L)	64.3
B) Geological parameters	
The portion of the node area covered by soft (quaternary) sediments, %, (Q)	28
C) Parameters of the lineament-and blocks geometry	
The highest rank of lineament in a node, (HR)	1
Number of lineaments forming a node, (NL)	2
Number of lineaments within a circle of 25km in radius (NLC)	5
Distance to the nearest 1st rank lineament, km, (D1)	11
Distance to the nearest 2nd rank lineament, km, (D2)	0
Distance to the nearest node, km, (Dn)	17
D) Morphological parameter (Mor) This parameter is equal to one of the following six values in accord with the morphology within each node: 1 mountain and mountain (m/m) 2 mountain and piedmont (m/pd) 3 mountain and plain (m/p) 4 mountain/piedmont/plain (m/pd/p) 5 piedmont and plain (pd/p) 6 piedmont (pd) 7 plain (p)	

Since the *CORA*-3 algorithm operates in a binary vector space, the measured values of the parameters are converted into binary vectors by discretization and coding procedure [10]. The range of the factual values of each parameter is divided into two or three parts by specifying one or two thresholds of discretization. One-threshold discretization considers two intervals of the factual values, which are converted into one binary component with the value 1 ("small") or 0 ("large"). Correspondingly, in two-threshold discretization the factual values of the parameters are converted into two binary components with the values 11 ("small"), 01 ("medium") or 00 ("large"). Table (2) displays the defined threshold of discretization for each parameter characterizing nodes in the study region.

5.3. Recognition of Nodes Prone to Earthquakes with $M \geq 6.0$ in the Alborz Region

The nodes have been classified by *CORA*-3. With $k_1 = 1$, $\bar{k}_1 = 2$, $k_2 = 10$, and $\bar{k}_2 = 1$, the algorithm selected eleven **D** traits and nine **N** traits, see Table (3), controlling the classification, when $\boldsymbol{D} = 0$. The classification shown in Figure (5) is the most stable among the others that were defined using different parameters of *CORA*-3 $k_1, \bar{k}_1, k_2, \bar{k}_2$, and $\boldsymbol{D}$. Of 134 nodes, 79 (58%) are classified **D** and 65 (49%) **N**. The recognized set of **D** nodes includes 30 objects originally in $\mathbf{D}_0$, 21 ones originally in $\mathbf{N}_0$, and 18 ones belonging to **X**. Figure (5) displays the recognized **D** nodes shown by scaled circles in 25km of radius.

6. Discussion and Conclusions

The recognition may be considered as successful because the nodes hosting earthquakes with $M \geq 6.0$ are recognized as **D** with only three exceptions: node 7, hosting the 1896 earthquake, and nodes 26 and 38 that accommodate very ancient events, the C1.800 and 958, respectively. Perhaps, the location and size of two last events defined by Berberian [4] should be revised.

A relatively big number of the recognized **D** nodes have no record so far of earthquakes with $M \geq 6.0$. Most of such nodes ate located in northern part of the Alborz. They sit on the first rank lineament that separate the Alborz and the Caspian lowland. According to "Liquefaction susceptibility map of Iran" [66], the Caspian coastal zone reveals the highest liquefaction susceptibility in the entire Alborz region. Due to this reason the intensity of earthquakes that are possible at seismogenic nodes in the northern Alborz can be significantly increased.

The parameters that make up **D** and **N** traits help to understand what distinguishes nodes prone to $M \geq 6.0$ from nodes of lower seismic potential (or aseismic ones). Seven parameters out of 13 ones tested in the
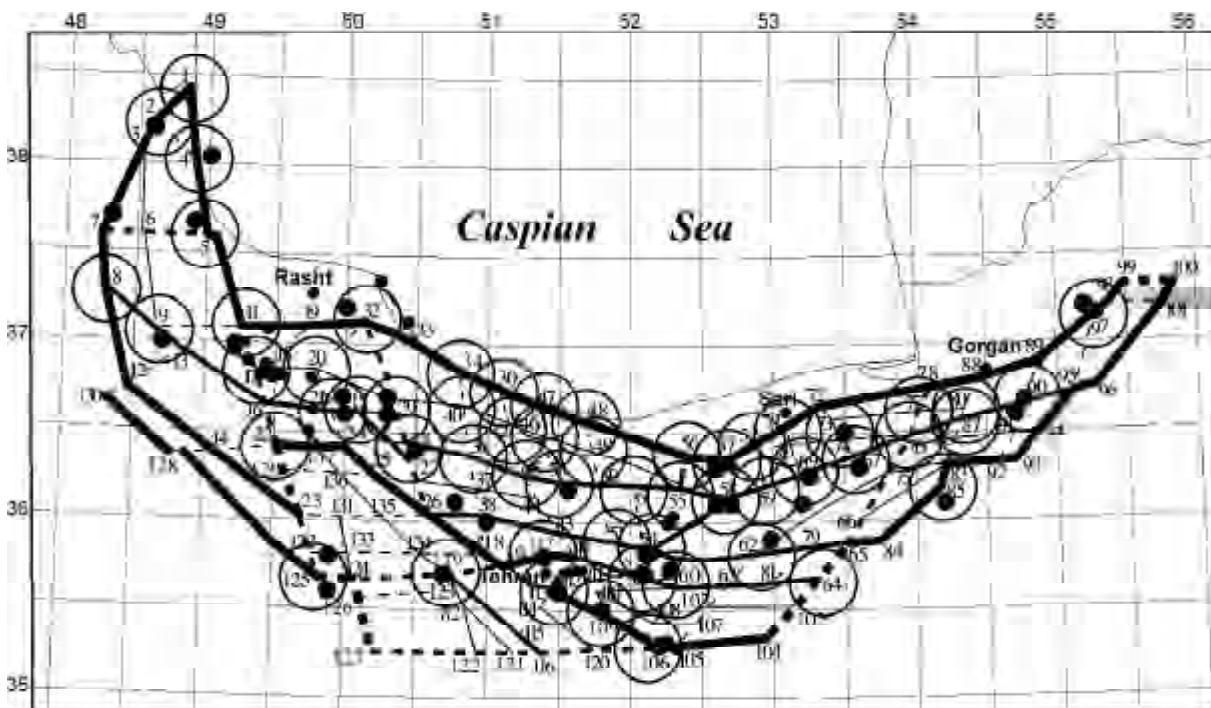

Figure 5. Recognized seismogenic nodes prone to M ≥ 6.0 earthquakes. Circles mark D nodes prone to earthquakes with M ≥ 6.0. The other symbols as in Figures (3) to (4).

Table 3. Recognized characteristic traits of D and N nodes in the Alborz region.

No.	Parameters						
	Hmin, m	DH m	DH/L	Mor	Q, %	D2, km	NL
Characteristic Traits of Class **D** (**D**-traits)							
1				m/pd/p *or* pd/p *or* pd *or*- p			> 2
2	≤ 1100					0	> 2
3			> 64.3	Other than m/m			> 2
4	> 1100		> 64.3				> 2
5	≤ 1100		≤ 64.3				> 2
6	> 1100	> 2379					> 2
7				m/m *or* m/pd *or* m/p	> 28		
8		> 2379	≤ 64.3			0	
9	≤ 1100		≤ 64.3			0	
10			> 64.3	Other than m/m	≤ 28		
11	≤ 1100	> 2379	≤ 64.3				
Characteristic Traits of Class **N** (**N**-trait)							
1					> 28	> 0	≤ 2
2				Other than m/m		> 0	≤ 2
3		≤2379				> 0	≤ 2
4	> 1100						≤ 2
5	> 1100					0	
6		≤2379		m/pd/p *or* pd/p *or* pd *or*- p			
7		≤2379		m/m *or* m/pd *or* m/p			
8	> 1100		≤ 64.3	Other than m/m			
9	> 1100	≤2379	≤ 64.3				

work, see Table (2) that compose the decision rule, see Table (3), are essential for recognition. These parameters are: *Hmin* (minimum topographic altitude), *DH* (difference in altitude between highest and lowest points at the node), *DH/L* (the relief gradient), *Mor* (morphology), *Q* (portion of soft sediments), *D*2 (the distance to the nearest second rank lineament), and *NL* (number of lineaments forming a node). From tectonic point of view morphometric *Hmin*, *DH*, and *DH/L*), morphological, and *Q* parameters indicate indirectly the contrasting neotectonic movements, while parameters *D*2 and *NL* characterize the intensity of crust fracturing at the nodes vicinities.

Characteristic traits No. 2, 5, 6, 9, 11, see Table (3), point out that **D** nodes are characterized by low elevation (*Hmin* ≤ 1100m). This indicates that **D** nodes possessing these traits associate with neotectonic subsidence on top of a background uplift dominated by the compressional tectonic regime in the Alborz region [36-37, 50, 60]. In other regions studied with this methodology, California, Greater Caucasus, and Dinarides [10, 24, 33, 61] subsidence was also found to be characteristic for the **D** nodes environments. Additional evidences corroborating the

importance of vertical movements at **D** nodes are large topographic gradient (*DH/L* > 64.3 in **D** traits Nos 3, 4, 10) and large relief energy (*DH* > 2379m in **D** traits Nos 6, 8, 11). On the contrary, the opposite intervals of these parameters are characteristic to **N** nodes, see Table (3).

The fragmentation of the crust is more pronounced near **D** than near **N** nodes. This is evident from parameter *NL*, which is included in six **D** traits and in four **N** traits, see Table (3). The large number of lineaments forming node (*NL* > 2) are characteristic for **D** nodes, while small value of the parameter dominate **N** nodes. This implies the intense crust fragmentation in the vicinity of **D** nodes. Recently, from the modeling of the block structure dynamics and seismicity, the intense fragmentation of the media has been established by Keilis-Borok et al [67] as a necessary precondition for the occurrence of most strong earthquakes.

The fact that *D*2 is apparently small for **D** and large for **N** implies that larger events originate at the boundaries of larger blocks. In general seismogenic nodes in the Alborz region are characterized by contrasting neotectonic movements and intense

fragmentation of the crust.

The study provides both practical and theoretical significant results. We can treat the obtained results as a zero approximation in predicting large earthquakes in the Alborz region. The work provides information on sites where earthquakes with $M \geq 6.0$ can occur. The recognition indicates high seismic potential of the Alborz region: a number of nodes where the target events have not been recorded till present have been recognized potential for their occurence.

References

1. Ambraseys, N.N. and Melville, C.P. (1982). "A History of Persian Earthquakes", Cambridge University Press, Cambridge, MA, 219.

2. Ahmadi, G., Mostaghel, N., and Nowroozi A.A. (1989). "Earthquake Risk Analysis of Iran - V: Probabilistic Seismic Risk for Various Peak Ground Accelerations", *Iranian J. Sci. Technol.*, B, 115-156.

3. Berberian, M. (1981). "Active Faulting and Tectonics of Iran, in: Zagros Hindu Kush Himalaya Geodynamic Evolution", Geodynamic Series, **3**, Edited by H.K. Gupta, and F.M. Delany, 33-69Am. Geophys. Union, Washington, DC and Geol. Soc. Am., Boulder, CO.

4. Berberian, M. (1994). "Natural Hazard and the First Earthquake Catalogue of Iran, 1: Historical Hazards in Iran Prior to 1900", 605p, IIEES, Thehran.

5. Nowroozi, A.A. (1976). "Seismotectonic Provinces of Iran", Bull. Seismol. Soc. Am., **66**, 1249-1276.

6. Shoja-Taheri, J. and Niazi, M. (1981). "Seismicity of the Iranian Plateau and Bordering Regions", Bull. Seismol. Soc. Am., **71**, 477-489.

7. Meletti, C., Patacca, E., and Scandone, P. (2000). "Construction of a Seismotectonic Model: The Case of Italy", PAGEOPH, **157**, 11-35.

8. Balassanian, S., Ashirov, T., Chelidze, T., et al (1999). "Seismic Hazard Assessment for the Caucasus Test Area, Annali di Geofisica, **42**(6), 1139-11.51.

9. Gelfand, I., Guberman, Sh., Keilis-Borok, V., Rantsman, E., and Izvekova, M. (1972). "Criteria of High Seismicity Determined by Pattern Recognition", *Tectonophysics*, **13**(1/4), 415-422.

10. Gorshkov, A., Kossobokov, V., and Soloviev, A. (2003). "Recognition of Earthquake Prone Areas, in Nonlinear Dynamics of the Lithosphere and Earthquake Prediction", Edited by V. Keilis-Borok and A. Soloviev, Heidelberg, 235-320.

11. Alexeevskaya, M.A., Gabrielov, A.M., Gvishiani, A.D., Gelfand, I.M., and Rantsman, E.Ya. (1977). "Formal Morphostructural Zoning of Mountain Territories", *J. Geophys.*, **43**, 227-233.

12. Talwani, P. (1988). "The Intersection Model for Intraplate Earthquakes", Seismol. Res. Lett., **59**, 305-310.

13. Talwani, P. (1999). "Fault Geometry and Earthquakes in Continental Interiors", *Tectonophysics*, **305**, 371-379.

14. Hudnut, K.W., Seeber, L., and Pacheo, J. (1989). Cross-Fault Triggering in the November 1987 Superstition Hills Earthquake Sequence", Southern California, Geophys. Res. Lett., **16**, 199-202.

15. Girdlet, R.W. and McConnell, D.A. (1994). "The 1990 to 1991 Sudan Earthquake Sequence and the Extent of the East African Rift System", Science, **264**, 67-70.

16. King, G. (1986). "Speculations on the Geometry of the Initiation a Termination Processes of Earthquake Rupture and Its Relation to Morphology and Geological Structure", Pure Appl. Geophys., **124**, 567-583.

17. Gabrielov, A., Keilis-Borok, V., and Jackson, D. (1996). "Geometric Incompatibility in a Fault System", *Proc. Natl. Acad. Sci. USA*, **93**, 3838-3842.

18. Gvishiani, A. and Soloviev, A.A. (1981). "Association of the Epicenters of Strong Earthquakes with the Intersection of Morphostructural Lines in South America", *Computational Seismology*, **13**, 42-47.

19. Cisternas, A., Godefroy, P., Gvishiani, A., Gorshkov, A., Kossobokov, V., Lambert, M., Rantsman, E., Sallantin, J., Saldano, H., Soloviev, A., and Weber, C. (1985). "A Dual Approach to Recognition of Earthquake Prone Areas in the Western Alps", Ann. Geophys., **3**(2), 249-270.

20. Bhatia, S.C., Chetty, T.R.K., Filimonov, M.,

Gorshkov, A., Rantsman, E., and Rao, M.N. (1992). "Identification of Potential Areas for the Occurrence of Strong Earthquakes in Himalayan Arc Region", *Proc. Indian Acad. Sci.* (Earth and Planet Sci.), **101**(4), 369-385.

21. Caputo, M., Keilis-Borok, V. Oficerova, E. Ranzman, E., Rotwain, I., and Solovieff, A. (1980). "Pattern Recognition of Earthquake-Prone Areas in Italy", Phys. Earth and Planet. Inter., **21**, 305-320.

22. Gelfand, I.M., Guberman, Sh.A., Izvekova, M.L., and Keilis-Borok, V.I., and Ranzman, E.Ya. (1973). "On Criteria of High Seismicity, Trans (Doklady)", Acad. Sci. SSSR, **202**(6), 1317-1320, 1972.

23. Gelfand, I.M., Guberman, Sh.A., Zhidkov, M.P., Kaletzkaya, M.S., Keilis-Borok, V.I., Ranzman, E.Ya., and Rotwain, I.M. (1974). "Recognition of Places where Strong Earthquakes May Occur, II. Four Regions in Asia Minor and South-Eastern Europe, 7-25, In Computer Analysis of Digital Seismic Data, Comput. Seismol. 7, edited by V. I. Keilis-Borok, Nauka, Moscow, (in Russian).

24. Gelfand, I., Guberman, Sh., Keilis-Borok, V. Knopoff, L., Press, F., Rantsman, E., Rotwain, I., and Sadovsky, A. (1976). "Pattern Recognition Applied to Earthquake Epicentres in California", Phys. Earth Planet. Inter., **11**, 227-283.

25. Gvishiani, A. and Soloviev, A. (1980). "On the Concentration of the Major Earthquakes Around the Intersections of Morphostructural Lineaments in South America, in Methods and Algorithms for Interpretation of Seismological Data", Edited by V.I. Keilis-Borok and A.L. Levshuin, 46-50 (eds), Nauka, Moscow, (in Russian).

26. Gvishiani, A.D. and Soloviev, A.A. (1984a). "Recognition of Places on the Pacific Coast of the South America where Strong Earthquakes May Occur", Earthquake Prediction Res., **2**, 237-242.

27. Gvishiani, A.D., Zhidkov, M.P., and Soloviev, A.A. (1984b). "Transfer of the High-Seismicity Criteria of the Andes Mountain Belt onto Kamchatka", Izv. Acad. Sci. SSSR, Phys. Earth, **1**, 20-26, (in Russian).

28. Gvishiani A., Gorshkov, A., Kossobokov, V., and Rantsman, E. (1986). "Morphostructures and Earthquake-Prone Areas in the Greater Caucasus", Izvestyia USSR Ac. Sci., Physics of the Earth., **9**, 15-23 (in Russian).

29. Gvishiani, A., Gorshkov, A., Cisternas, A. Rantsman, E., and Soloviev, A. (1988). "Identification of Earthquake-Prone-Areas in the Regions of Moderate Seismicity", 189p, Nauka, Moscow, (in Russian).

30. Gorshkov, A., Zhidkov, M., Rantsman, E., and Tumarkin, A. (1991). "Morphostructures of the Lesser Caucaus and Sites of Earthquakes, M ≥ 5.5, Izvestyia USSR", Ac. Sci., Physics of the Earth., **6**, 30-38 (in Russian).

31. Gorshkov, A., Kuznetsov, I., Panza, G., and Soloviev, A. (2000). "Identification of Future Earthquake Sources in the Carpatho-Balkan Orogenic Belt Using Morphostructural Criteria", PAGEOPH, **157**, 79-95.

32. Gorshkov, A.I., Panza, G.F., Soloviev, A.A., and Aoudia, A. (2002). "Morphostructural Zonation and Preliminary Recognition of Seismogenic Nodes Around the Adria Margin in Peninsular Italy and Sicily", *JSEE*, **4**(1), 1-24.

33. Gorshkov, A.I., Panza, G.F., Soloviev, A.A., and Aoudia, A. (2004). "Identification of Seismogenic Nodes in the Alps and Dinarides", Bollettino Della Societa Geologica Italiana, **123**, 3-18.

34. Philip, H., Cisternas, A., Gvishiani, A., and Gorshkov, A. (1989). "The Caucasus: An Actual Example of the Initial Stages of a Continental Collision", *Tectonophysics*, **161**, 1-21.

35. McKenzie, D.P. (1972). "Active Tectonics of the Mediterranean Region", *Geophysical Journal of the Royal Astronomical Society*, **30**, 109-185.

36. Allen, M.B., Ghassemi, M.R., Shahrabi, M., and Qorashi, M. (2003). "Accommodation of Late Cenozoic Oblique Shortening in the Alborz Range, Northern Iran", *Journal of Structural Geology*, **25**, 659-672.

37. DeMets, C., Gordon, R.G., Argus, D.F., and Stein, S. (1990). "Current Plate Motions", *International Journal of Geophysics*, **101**, 425-478.

38. Hempton, M.R. (1987). "Constraints on Arabian

Plate Motion and Extensional History of the Red Sea", *Tectonics 6*, 687-705.

39. Alavi, M. (1996). "Tectonostratigraphic Synthesis and Structural Style of the Alborz Mountain System in Northern Iran", *J. Geodynamics*, **21**(1), 1-33.

40. Dewey, J.F., Holdsworth, R.E., and Strachan, R.A. (Eds.) (1998). "Transpression and Transtension Zones", *Geological Society Special Publication*, **135**, 1-14.

41. Berberian, M. and Yeats, R.S. (1999). "Patterns of Historical Earthquake Rupture in the Iranian Plateau", Bull. Seism. Soc. Am., **89**, 120-139.

42. Stocklin, J. (1974). "Northern Iran: Alborz Mountains", Geol. Soc. Lon. Special Publication No. 4, 213-234.

43. Berberian, M. and King, G. (1981). "Towards a Paleogeography and Tectonic Evolution of Iran", *Can. J. Earth Sci.*, **18**, 210-265.

44. Berberian, M. (1983). "The Southern Caspian: A Compressional Depression Floored by a Trapped, Modified Oceanic Crust", *Can. Journal Earth Sci.*, **20**, 163-183.

45. Jackson, J., Priestly, K., Allen, M., and Berberian, M. (2002). "Active Tectonics of the South Caspian Basin", *Geophys. J. Int.*, **148**, 214-245.

46. Vernat, P., Nilforoushan F., and Hatzfeld, D. (2004). "Present-Day Crustal Deformation and Plate Kinematics in Middle East Constrained by GPS Measurements in Iran and Northern Oman", *Geophysical Journal International*, **157**, 381-398.

47. Jackson, J. and Fitch, Th.J. (1979). "Seismotectonic Implications of Relocated Aftershock Sequence in Iran and Turkey", *Geophys. J. of the Royal Astr. Soc.*, **57**, 209-229.

48. Khain, V.E. (2000). "Tectonics of Continents and Oceans", 500p, Scientific World, Moscow, (in Russian).

49. Sengor, A.M.C. (1990). "A New Model for the Late Paleozoic-Mesozoic Evolution of Iran and Implications for Oman, In: The Geology and Tectonics of the Oman Region", Special Publication No. 49, Edited by Robertson, A. et al, 797-831.

50. Trifonov, V. (1983). "Late Quaternary Tectonogenesis", Moscow: Nauka, 240p, (in Russian).

51. Sadovsky, M.A., Golubeva, T.V., Pisarenko, V.F., and Shnirman, M.G. (1984). "Characteristic Dimensions of Rock and Hierarchical Properties of Seismicity", Izv. Acad. Nauk SSSR, Phys. Solid Earth., **20**, 87-96,

52. Keilis-Borok, V.I. (1990). "The Lithosphere of the Earth as a Nonlinear System with Implications for Earthquake Prediction", Rev. Geophys., **28**, 19-34.

53. Krasny, L.I. (1984). "The Global System of Geoblocks, Nedra, Moscow, (in Russian), 224p.

54. Bird, P. (2003). "An Updated Digital Model of Plate Boundaries", *Geochemistry Geophysics Geosystems*, **4**(3), 1027.

55. Keilis-Borok, V.I. (2003). "Fundamentals of Earthquake Prediction: Four Paradigms. In Nonlinear Dynamics of the Lithosphere and Earthquake Prediction", Edited by V. Keilis-Borok and A. Solovoiev, 1-68, Heidelberg.

56. Hodgson, R.A. (1974). "Review of Significant Early Studies in Lineament Tectonics", *Proc. of the First International Conference on the New Basement Tectonics*, R. Hodgson, S. Gay, J. Benjamins, eds., Utah Geological Association Publication No. 5, 1-10.

57. Hobbs, W.H. (1911). "Repeating Patterns in the Relief and the Structure of the Land", B.G.S.A., **22**, 123-176.

58. Milanovsky, E. (1968). "Neotectonics of the Caucasus", Nedra, Moscow, (in Russian), 482p.

59. Linzer, H.G., Rautschbacher, L., and Frish, H.W. (1995). "Transpressional Collision Structures in the Upper Crust: The Fold-Thrust Belt of the Northern Calcareous Alps", *Tectonophysics*, **242**, 41-61.

60. Gvishiani, A., Gorshkov, A. Kossobokov, V., Cisternas, A., Philip, H., and Weber, C. (1987). "Identification of Seismically Dangerous Zones in the Pyrenees", Annales Geophysicae, **5B**(6), 681-690.

61. Hessami, Kh., Jamali, F., and Tabassi, H. (2003). "Major Active Faults of Iran", IIEES, Tehran.

62. Wells, D.L. and Coppersmith, K.J. (1994). "New Empirical Relationships Among Magnitude, Rupture Length, Rupture Width, and Surface Displacement", Bull. Seism. Soc. Am., **84**, 974-1002.

63. Engdahl, E.R., Van Der Hilst, R., and Buland, R. (1998). "Global Teleseismic Earthquake Relocation with Improved Travel Times and Procedures for Depth Determination", Bull. Seism. Soc. Am., **88**, 722-743.

64. Kondorskaya, N., Gorbunova, I., Kireev, I., and Vandysheva, N. (1993). "On the Unified Earthquake Catalog of North Euroasia", In Seismisity and Seismic Zoning of North Eurasia, Edited by V. Ulomov, IPE, Moscow, 70-79.

65. Shebalin, N.V. and Tatevosian, R.E. (1997). "Catalogue of Large Historical Earthquakes of the Caucasus, in: Historical and Prehistorical Earthquakes in the Caucasus", Edited by D. Giardini and S. Balassanian, NATO ASI Series, 2. Environment, **28**, Kluwer Academic Publishers: Dordrecht/Boston/London, 201-232.

66. Liquefaction Susceptibility Map of Iran (2000). IIEES, Tehran, 1:2,000,000.

67. Keilis-Borok, V.I., Rotwain, I.M., and Soloviev, A.A. (1997). "Numerical Modeling of Block Structure Dynamics: Dependence of a Synthetic Earthquake Flow on the Structure Separateness and Boundary Movements", *J. of Seismology*, **1**(2), 151-160.